blood advances

American Society of Hematology
2021 L Street NW, Suite 900,
Washington, DC 20036
Phone: 202-776-0544 | Fax 202-776-0545
bloodadvances@hematology.org

O-glycan determinants regulate VWF trafficking to Weibel-Palade bodies

Tracking no: ADV-2023-012499R2

Ellie Karampini (Royal College of Surgeons In Ireland, Ireland) Dearbhla Doherty (Royal College of Surgeons in Ireland (RCSI), Dublin, Ireland, Ireland) Petra Bürgisser (Erasmus MC, University Medical Center Rotterdam, Netherlands) Massimiliano Garre (Royal College of Surgeons Ireland, Ireland) Ingmar Schoen (Royal College of Surgeons Ireland, Ireland) Stephanie Elliott (Royal College of Surgeons in Ireland, Ireland) Ruben Bierings (Erasmus University Medical Center, Netherlands) James O'Donnell (Royal College of Surgeons in Ireland, Ireland)

Abstract:
Von Willebrand factor (VWF) undergoes complex post-translational modification within endothelial cells (EC) prior to secretion. This includes significant N- and O-linked glycosylation. Previous studies have demonstrated that changes in N-linked glycan structures significantly influence VWF biosynthesis. In contrast, although abnormalities in VWF O-linked glycans (OLG) have been associated with enhanced VWF clearance, their effect on VWF biosynthesis remains poorly explored. Herein, we report a novel role for OLG determinants in regulating VWF biosynthesis and trafficking within EC. We demonstrate that alterations in OLG (notably reduced terminal sialylation) lead to activation of the A1 domain of VWF within EC. In the presence of altered OLG, VWF multimerization is reduced and Weibel-Palade body (WPB) formation significantly impaired. Consistently, the amount of VWF secreted from WPB following EC activation was significantly reduced in the context of O-glycosylation inhibition. Finally, altered OLG on VWF not only reduced the amount of VWF secreted following EC activation, but also affected its hemostatic efficacy. Notably, VWF secreted following WPB exocytosis consisted predominantly of low molecular weight multimers and the length of tethered VWF string formation on the surface of activated ECs was significantly reduced. In conclusion, our data therefore support the hypothesis that alterations in O-glycosylation pathways directly impact VWF trafficking within human EC. These findings are interesting given that previous studies have reported altered OLG on plasma VWF (notably increased T antigen expression) in patients with von Willebrand disease.

Conflict of interest: COI declared - see note

COI notes: J.S.O.D has served on the speaker's bureau for Baxter, Bayer, Novo Nordisk, Sobi, Boehringer Ingelheim, Leo Pharma, Takeda and Octapharma. He has also served on the advisory boards of Baxter, Sobi, Bayer, Octapharma CSL Behring, Daiichi Sankyo, Boehringer Ingelheim, Takeda and Pfizer. J.S.O.D has also received research grant funding awards from 3M, Baxter, Bayer, Pfizer, Shire, Takeda, 3M and Novo Nordisk. The remaining authors have no conflict-of-interests to declare.

Preprint server: No;

Author contributions and disclosures: E.K. and J.S.O.D conceived the study and contributed to data collection and interpretation. D.D., P.B., M.G. and S.E assisted with data collection. I.S. assisted with image analysis. E.K., D.D., P.B., M.G., S.E., R.B., and J.S.O.D. contributed to the literature review, final draft writing, and critical revision and approved the final version of the manuscript. All the authors have participated sufficiently in this work, take public responsibility for the content, and have made substantial contributions to this research.

Non-author contributions and disclosures: No;

Agreement to Share Publication-Related Data and Data Sharing Statement: Emails to the corresponding author.

Clinical trial registration information (if any):

O-glycan determinants regulate VWF trafficking to Weibel-Palade bodies.

Ellie Karampini[1], Dearbhla Doherty[1], Petra E Bürgisser[2], Massimiliano Garre[3], Ingmar Schoen[1], Stephanie Elliott[1], Ruben Bierings[2] and James S. O'Donnell[1,4].

[1] Irish Centre for Vascular Biology, School of Pharmacy and Biomolecular Sciences, Royal College of Surgeons in Ireland, Dublin, Ireland.
[2] Department of Hematology, Erasmus MC, Rotterdam, the Netherlands
[3] Super-Resolution Imaging Consortium, Department of Chemistry, Royal College of Surgeons in Ireland, Dublin, Ireland
[4] National Coagulation Centre, St James's Hospital, Dublin, Ireland

Running Title:	**O-glycans influence VWF trafficking**
Abstract word count:	**240**
Text word count:	**4078**
Figure count:	**7**
Reference count:	**66**
Scientific Section:	**THROMBOSIS AND HAEMOSTASIS**

Editorial correspondence should be addressed to:
Prof. James O'Donnell
Irish Centre for Vascular Biology, Royal College of Surgeons in Ireland,
Ardilaun House, 111 St Stephen's Green, Dublin 2, Ireland.
Tel +353 (1) 402 2209; e-mail jamesodonnell@rcsi.ie

Presented in abstract form of oral presentations at the 30th International Society on Thrombosis and Haemostasis Congress, London, UK, July 2022 and the 31st International Society on Thrombosis and Haemostasis Congress, Montreal, Canada, June 2023.

Data Sharing Statement – data available for sharing by email request to the corresponding author.

KEY POINTS

1. VWF O-glycans critically influence VWF biosynthesis and trafficking into Weibel-Palade bodies in human endothelial cells.
2. O-glycan inhibition leads to VWF A1 domain activation and formation of significantly smaller Weibel-Palade bodies.

ABSTRACT

Von Willebrand factor (VWF) undergoes complex post-translational modification within endothelial cells (EC) prior to secretion. This includes significant N- and O-linked glycosylation. Previous studies have demonstrated that changes in N-linked glycan structures significantly influence VWF biosynthesis. In contrast, although abnormalities in VWF O-linked glycans (OLG) have been associated with enhanced VWF clearance, their effect on VWF biosynthesis remains poorly explored. Herein, we report a novel role for OLG determinants in regulating VWF biosynthesis and trafficking within EC. We demonstrate that alterations in OLG (notably reduced terminal sialylation) lead to activation of the A1 domain of VWF within EC. In the presence of altered OLG, VWF multimerization is reduced and Weibel-Palade body (WPB) formation significantly impaired. Consistently, the amount of VWF secreted from WPB following EC activation was significantly reduced in the context of O-glycosylation inhibition. Finally, altered OLG on VWF not only reduced the amount of VWF secreted following EC activation, but also affected its hemostatic efficacy. Notably, VWF secreted following WPB exocytosis consisted predominantly of low molecular weight multimers and the length of tethered VWF string formation on the surface of activated ECs was significantly reduced. In conclusion, our data therefore support the hypothesis that alterations in O-glycosylation pathways directly impact VWF trafficking within human EC. These findings are interesting given that previous studies have reported altered OLG on plasma VWF (notably increased T antigen expression) in patients with von Willebrand disease.

KEYWORDS

Von Willebrand factor, von Willebrand disease, Glycosylation, Weibel-Palade bodies,

INTRODUCTION

Von Willebrand factor (VWF) is a large multimeric plasma sialo-glycoprotein that plays critical roles in normal haemostasis.[1] Under normal conditions, in vivo expression of VWF is limited to endothelial cells (EC) and megakaryocytes.[2,3] Prior to secretion, VWF undergoes complex post-translational modification that includes significant glycosylation.[3,4] N-linked glycosylation begins in the endoplasmic reticulum, through addition of high-mannose oligosaccharide chains onto 12 sites in the VWF monomer.[5] Following transport to the Golgi apparatus, these initial N-linked glycan (NLG) structures undergo further modification, leading to the formation of complex branching carbohydrate chains.[6] O-linked glycosylation of the VWF dimer also takes place in the Golgi, leading to the formation of 10 O-linked glycan (OLG) chains. O-glycosylation is initiated by addition of GalNAc residues onto specific serine or threonine residues, leading to formation of the precursor Tn antigen (GalNAcα1-Ser/Thr).[7,8] This initial O-glycan is then extended by core 1 β3-galactosyltransferase 1 (C1GALT1) which catalyzes addition of galactose residues to convert Tn into T antigens (Gal1-3βGalNAcα1-Ser/Thr) (**Fig. 1A**).[9] Sialylated core 1 T antigens constitute the predominant OLG on human VWF.[10,11] Importantly, eight of the OLG chains on VWF are present in two clusters located either side of the A1 domain (Cluster1; T1248, T1255, T1256, S1263 and Cluster 2; T1468, T1477, S1486, T1487).[12] Although most N- and O-glycans of VWF are capped by sialic acid,[13] covalently linked ABO(H) blood group carbohydrate determinants are also present as terminal sugar residues on a proportion of both the N-linked (13%), and O-linked (1%) chains.[14]

Previous studies have demonstrated that the NLG and OLG structures on VWF (notably terminal sialylation and ABO(H) blood group determinants) play important roles in regulating susceptibility to ADAMTS13 proteolysis[15-18] and in vivo clearance.[19-24] In addition, specific NLG structures on VWF have also been shown to influence VWF biosynthesis within EC.[25,26] For example, EC treatment with tunicamycin inhibited precursor NLG sugar chain attachment to VWF, which in turn led to impaired dimerization.[25] Consequently, VWF secretion was ablated and intracellular VWF levels were significantly reduced.[25] Similarly, EC incubation with castanospermine (CSP) inhibited glucosidase activity in the ER and thus NLG chain development on VWF.[26] Unlike tunicamycin, CSP treatment did not prevent dimerization, but nonetheless significantly attenuated VWF secretion.[26]

There are conflicting data regarding whether O-glycan carbohydrates influence VWF biosynthesis.[27-29] Using site-directed mutagenesis, Nowak *et al.* reported no significant difference in secreted recombinant VWF (rVWF) levels for a range of O-glycan variants expressed in HEK293T cells compared to wild type (VWF-WT).[27] Importantly however, previous studies have shown that rVWF expression in HEK293**T** cells does not lead to Weibel-Palade body (WPB) formation.[30] Conversely, Badirou *et al.* found that expression of murine rVWF missing all OLG was significantly reduced in COS-7 cells compared to wild type VWF (WT-VWF).[28] In keeping with the concept that OLG may impact VWF biosynthesis, a recent GWAS study implicated OLG processing genes in determining VWF biosynthesis.[31] Furthermore, previous studies also demonstrated that OLG structures influence mucin biosynthesis and in particular intracellular trafficking.[32]

In this study, we therefore investigated the hypothesis that OLG may specifically impact VWF trafficking in EC capable of producing WPB.

MATERIALS AND METHODS

Cell culture

Human umbilical vein endothelial cells (HUVEC) were cultured in endothelial cell growth medium (PromoCell, Heidelberg, Germany) supplemented with 18% heat inactivated fetal bovine serum (FBS) and 1% penicillin and streptomycin (Pen-Strep). All experiments were performed using HUVEC between passages 3 and 5. Human embryonic kidney 293 (HEK293) cells were cultured in Dulbecco′s Modified Eagle′s Medium (Merck, Darmstadt, Germany) supplemented with 10% FBS and 1% Pen-Strep. HEK293 cells were used before passage 20.

OLG inhibition with Benzyl-N-acetyl-galactosaminide (GalNAc-O-benzyl; BG) and Itraconazole (ITZ)

HUVEC were plated on gelatin coated plates and allowed to reach confluency. Confluent monolayers were treated with 2mM BG (Merck) or vehicle (DMSO) for 72 hours. After 72 hours, HUVEC were either fixed, or the media was changed to allow collection of steady-state secreted VWF into the supernatant. To determine intracellular VWF levels, HUVEC were lysed in PBS containing 1% Triton in the presence of proteases inhibitors on ice. Similar to BG treatment, HUVEC monolayers were treated with 2 μM ITZ (Merck) for 72 hours. VWF:Ag and VWF:CB activity levels in cell supernatants and lysates were determined using ELISA as previously described.[33] VWF multimers were analyzed by agarose gel electrophoresis as before.[34] Secreted angiopoietin-2 (Angpt-2) levels in HUVEC supernatant were determined by commercial ELISA (Bio-Techne, R&D systems) following the manufacturer's instructions.[35]

Western blot analysis

BG-treated, ITZ-treated or control cell lysate and supernatant samples were diluted with SDS sample buffer and DTT prior to boiling at 95°C for 10 minutes. Boiled samples were loaded in Bis-Tris 4-12% gels (Invitrogen, ThermoFisher Scientific, Waltham, MA USA) and separated for 40 minutes. Proteins were transferred onto a nitrocellulose membrane and blocked with 5% BSA-PBS-Tween 0.1% for 1 hour. Membranes were then probed with primary anti-VWF (1:1000, DAKO Agilent Technologies, Santa Clara, CA, US), anti-GAPDH (1:2500, Abcam, Cambridge, UK), anti-C1GALT1 (1:1000, Santa Cruz Biotechnology, Dallas, TX, US) or anti α-tubulin (1:2500, Abcam Cambridge, UK) antibodies overnight at 4°C and subsequently incubated with HRP-conjugated secondary antibodies. Blots were visualized with enhanced chemiluminescence (ECL) substrates in an AmershamTM 680 Imager.

Lectin analysis of VWF OLG determinants

VWF glycans were assessed using specific lectin ELISAs as previously described.[23] In brief, PolySorb flat bottom plates were coated using deglycosylated polyclonal anti-VWF 1:250 (Dako, Agilent Technologies). Non-specific binding was blocked with Protein-Free Blocking Buffer™ (Thermo Fisher Scientific, UK). Conditioned media from control or BG-treated HUVEC were diluted in PBS and loaded onto the plate and incubated for 2 hours at 37°C. Biotinylated lectins Peanut agglutinin (PNA) (1µg/ml) or *Maackia amurensis* lectin *II* (MAL-II) (2.5µg/ml) (both Vector Laboratories, UK) were diluted in PBS-T and incubated for 1 hour at 37°C. Lectin binding was detected with high sensitivity streptavidin–horseradish peroxidase (Pierce, Thermo Fisher Scientific,

UK) and subsequent incubation with substrate 3,3',5,5'-Tetramethylbenzidine (TMB; R&D Systems, UK). The reaction was subsequently stopped with 1M H_2SO_4. Absorbance was read at 450nm using a SpectraMax Reader. All ELISAs were repeated three times and dilutions were measured per duplicate.

Immunofluorescence microscopy

Paraformaldehyde (PFA) fixed glass coverslips of control and BG-treated cells were permeabilized with 0.1% Triton X-100 (in PBS containing 0.05% sodium azide (NaN3) and 0.01% BSA) for 15 minutes and blocked with 3% BSA in PBS for 45 minutes. Coverslips were then incubated in a humidifying chamber with primary antibodies for 1 hour at room temperature. Subsequently, the coverslips were incubated in a humidifying chamber with fluorescently labelled secondary antibodies 1:1000, Invitrogen, ThermoFisher Scientific) for 1 hour at room temperature in the dark. Coverslips were mounted onto glass slides and images acquired using a Leica Stellaris 8 STED 3D/Falcon/confocal system (Leica microsystems, Ashbourne, Ireland) with Leica HC PL APO CS2 100X/1.40 oil immersion objective. WPB morphology (> 8,000 per treatment) in ECs were assessed with an automated script in Image J/ Fiji, where the WPB length was measured by Feret's diameter (the longest distance between any two points in the selection boundary) and circularity assessed by the formula $4\pi * (\frac{area}{perimeter^2})$. Nanobodies directed against the activated VWF-A1 domain and the VWF-A3 domain were kindly provided by Dr. P.J. Lenting (Paris, France). Nanobodies were conjugated to Alexa-488 (nano-active A1) and Alexa-647 (nano-A3) and used as previously described.[36]

Transient expression of VWF OLG variants in HEK293 cells

The expression vector pcDNA-VWF encoding recombinant full-length human VWF has previously been described.[27] Additional rVWF variants were prepared by site-directed alanine mutagenesis of individual serine and threonine residues. These included VWF-ΔC1 in which the N-terminal cluster 1 OLG were removed (containing T1248A, T1255A, T1256A, S1263A) and VWF-ΔC2 in which the C-terminal cluster 2 OLG (containing T1468A, T1477A, S1486A, T1487A) flanking the VWF-A1 domain were removed. Finally, a VWF-ΔC1+ΔC1 variant missing both OLG clusters (containing T1248A, T1255A, T1256A, S1263A, T1468A, T1477A, S1486A, T1487A) was also generated as previously described in detail.[27] These variants were kindly provided by Dr. T.A. McKinnon (Imperial College London, UK). All rVWF variants were transiently expressed in HEK293 cells. In brief, HEK293 were grown to confluence and then transfected using TurboFect (Thermofisher). 24 hours later, the media was changed back to DMEM containing 10% FBS and cells allowed to express the rVWF variants for a further 48 hours before pseudo WPB formation was assessed.

Histamine-induced VWF release and string formation under shear

BG-treated or control HUVEC were washed and starved for 15 minutes in release medium (RM: M199 containing 0.2% BSA) prior to stimulation assay. After washing, cells were incubated in RM supplemented with histamine (100 μM final concentration; Merck) for 30 minutes. VWF:Ag and VWF:CB activity in the supernatant were then assessed by ELISA as detailed above.

To assess VWF string formation, BG-treated and control HUVEC were plated on gelatin-coated 6 channel µ-slide (Ibidi). After 24 hours, the HUVEC were activated under flow (1.5 ml/min) with histamine (100 µM). Tethered VWF strings on the HUVEC cell surface were visualized by flowing over washed platelets in brightfield (Axiovert200, Zeiss) at 37°C. Whole blood samples were collected from healthy consenting volunteers in accordance with RCSI research ethics (REC1391 and REC1504) and the Declaration of Helsinki. Washed platelets were obtained from whole blood of healthy blood donors as previously described.[37] Alternatively, tethered VWF strings were also visualized using fluorescently labelled anti-VWF antibodies (Zenon labelling kit, Thermofisher) in the green channel using a Leica Stellaris 8 STED 3D/Falcon/confocal system (Leica microsystems) and Okolab incubation system with temperature (37°C) and CO_2 (5%) control.

Data Presentation and Statistical Analysis

All images were analyzed using ImageJ/ Fiji. Graphpad Prism 10.0 was used to plot and analyze data. Data are presented as mean and standard deviation (SD) unless stated otherwise. Data that are normally distributed are tested for significance by a Student's t-test (or one-way AVOVA for three or more conditions). Data that are not normally distributed are tested for significance by a Mann-Whitney t-test (or Kruskal-Wallis for three or more conditions). A p-value below 0.05 was considered significant.

Data Availability - The data that support the findings of this study are available from the corresponding author upon reasonable request.

RESULTS

BG treatment of HUVECs alters VWF O-linked glycosylation.

Benzyl-N-acetyl-galactosaminide (GalNAc-*O*-benzyl; BG) has been shown to inhibit key steps in OLG development (**Fig. 1A**).[38,39] To investigate whether OLG influences VWF biosynthesis in human EC, HUVEC were treated with BG. Consistent with reduced O-linked glycosylation, a reduction in molecular weight was observed for VWF in cell lysates, and for VWF secreted into the supernatant from BG-treated HUVEC compared to untreated controls (**Fig. 1B**). Since previous studies demonstrated that BG treatment resulted in reduced sialylation of mucin OLG,[38] the effects of BG on VWF OLG chains were assessed using lectin ELISAs. In keeping with the mucin studies, treatment of HUVEC with BG resulted in significantly ($p<0.001$) reduced *Maackia amurensis* lectin *II* (MAL-II) binding to secreted VWF, consistent with a reduction in terminal α2-3 sialylation (**Fig. 1C**). Furthermore, BG-treatment was also associated with a significant ($p=0.0063$) increase in binding of Peanut agglutinin (PNA) lectin (which binds to non-sialylated core 1 glycans) to secreted VWF compared to untreated controls (**Fig. 1D**). Together, these data demonstrate that BG-treatment of EC directly affects VWF O-glycosylation, resulting in a partial reduction in terminal α2-3 linked sialylation and a consequent increase in T-antigen expression.

O-linked sialylation influences VWF secretion and alters WPB morphology.

Previous studies investigating a putative role for OLG in regulating VWF biosynthesis were performed in cells that did not form WPB storage organelles.[27,28] Consequently, we next investigated whether alterations in O-linked sialylation influenced VWF

trafficking in WPB-containing human EC. Importantly, incubation with BG was associated with a significant increase (p=0.0013) in unstimulated VWF secretion from HUVEC (**Fig. 2A**). In contrast, no effect on steady state intracellular VWF concentration in HUVEC lysates was observed (**Fig. 2B**). To further investigate the mechanisms through which OLG influence VWF synthesis and trafficking within human EC, immunofluorescence microscopy was used to assess WPB morphology. In contrast to normal HUVEC, WPB morphology was markedly altered in HUVEC incubated with BG compared to controls (**Fig. 2C**). In particular, inhibition of O-linked sialylation resulted in the formation of WPB that were significantly shorter (p<0.0001) **(Fig. 2D)** and rounder (p<0.0001) **(Fig. 2E)** compared to the elongated cigar-shaped WPB seen in control HUVEC. Collectively, these results indicate that alterations in O-linked glycosylation significantly impact WPB formation and VWF secretion in EC.

C1GALT1 influences VWF O-linked glycan determinants and WPB morphology.

C1GALT1 plays a key role in T antigen synthesis by catalyzing transfer of galactose residues onto precursor Tn antigens (**Fig. 3A**).[40,41] Itraconazole (ITZ) has been shown to inhibit T antigen formation in cancer cell lines by targeting C1GALT1 for proteasomal degradation.[40,41] To further evaluate the effects of OLG in regulating VWF biosynthesis, HUVEC were next treated with ITZ. Consistent with the notion that ITZ reduces C1GALT1 in other cell types,[41] we observed markedly reduced C1GALT1 expression in ITZ-treated HUVECs compared to untreated controls (**Fig. 3B**). Similar to BG, a reduction in molecular weight was also observed for (i) VWF in cell lysates and (ii) VWF secreted into the supernatant from ITZ-treated HUVEC compared to untreated controls

(**Fig. 3C**). In agreement with our BG observations, ITZ-treatment was associated with a significant increase ($p<0.0001$) in unstimulated basal VWF secretion from HUVEC (**Fig. 3D**). Moreover, immunofluorescence microscopy confirmed that WPB morphology was markedly altered in HUVEC incubated with ITZ compared to controls (**Fig. 3E**), with WPB significantly reduced in length ($p<0.0026$) compared to WPB in untreated control HUVEC **(Fig. 3F)**. Interestingly, ITZ treatment had a more marked effect on unstimulated VWF secretion but a less significant effect on WPB formation when compared to BG treatment.

Altogether, these observations further support the hypothesis that OLG truncations significantly influence WPB length and VWF secretion.

Effects of VWF OLG truncation on Golgi morphology and WPB cargo storage.

Previous studies have shown that the length of WPB is determined before they bud off from the *trans*-Golgi network (TGN).[42,43] In addition, Ferraro *et al* demonstrated that normal Golgi ribbon architecture was needed for packing of VWF quanta into nascent WPBs.[42] Consequently, unlinking of the Golgi into ministacks led to the formation of short WPBs.[42-44] To investigate whether OLG truncation induced unlinking of the Golgi, we next performed immunofluorescent co-staining of TGN and VWF in control and BG-treated cells. No significant alteration in Golgi morphology was observed in control and BG-treated cells (**Fig. 4A**). In BG-treated cells that were producing short WPBs, the Golgi appeared continuous, indicating that the BG treatment does not affect the Golgi homeostasis. Angiopoietin-2 (Angpt-2) is another EC glycoprotein stored within WPB and secreted following EC activation.[45,46] Despite the small and stubby WPB formed in

BG-treated HUVEC, we observed that Angpt-2, which does not have any known OLG sites, was still recruited into WPB in these cells (**Fig. 4B**). Importantly however, consistent with enhanced unstimulated VWF secretion levels, a significant (p=0.0062) increase in basal Angpt-2 secretion was also seen following HUVEC incubation with BG (**Fig. 4C**). These data suggest that alterations in VWF OLG leading to alterations in WPB morphology may have additional biological effects by affecting secretion of other WPB cargo components.

O-glycan clusters in VWF impact pseudo-WPB morphology.

To confirm that the effects of BG and ITZ were modulated by changes in VWF O-glycan structures, a series of recombinant VWF OLG mutants were examined. These included rVWF in which the N-terminal (VWF-ΔC1) and C-terminal (VWF-ΔC2) OLG clusters at either side of the VWF A1 domain were removed using alanine mutagenesis of serine and threonine residues as previously described (**Fig. 5A**).[27] In addition, a rVWF variant lacking both OLG clusters (VWF-ΔC1+ΔC2)[27] was also studied. Nowak *et al* previously reported that expression and secretion of these variants was not significantly different to wild-type VWF.[27] In contrast to previous studies,[27,28] HEK293 cells were used for these expression studies as these have been shown to produce pseudo-WPB following rVWF expression.[30] Consistent with our OLG inhibitor data, expression of VWF-ΔC1, VWF-ΔC2 and VWF-ΔC1+ΔC2 in HEK293 cells all resulted in the formation of short and stubby WPBs (**Fig. 5B & 5C**). Interestingly, the magnitude of this effect on WPB morphology was most marked for VWF-ΔC1+ΔC2 in which both OLG clusters either side of the A1 domain were absent (**Fig. 5B & 5C**). In addition, loss of

the N-terminal OLG cluster (VWF-ΔC1) had a significantly greater effect on pseudo-WPB morphology compared to removal of the C-terminal OLG cluster (VWF-ΔC2) (p=0.014) (**Fig. 5C**).

In keeping with the HUVEC data, BG-treatment of HEK293 transfected with wild type VWF (VWF-WT) resulted in pseudo-WPB that were significantly (p=0.0125) reduced in length compared to untreated controls (**Fig. 5D**). Furthermore, this BG-induced reduction in pseudo-WPB size was similar to VWF-ΔC1+ΔC2 expressed in HEK293 cells. Finally, BG treatment of HEK293 cells producing VWF-ΔC1+ΔC2 had no additional effect in reducing WPB size (**Fig. 5E**). Together, our findings demonstrate for the first time that OLG determinants on VWF play a critical role in regulating WPB size.

OLG inhibition leads to VWF-A1 domain activation and reduced HMW multimers.

Loss of O-linked sialylation has recently been reported to result in A1 domain activation mediated via destabilization of the flanking autoinhibitory module (AIM).[47] Consequently, we next studied the effect of BG-induced OLG inhibition on A1 domain activation using a specific nanobody towards activated A1 (**Fig. 6A**).[48] Interestingly, intracellular A1 domain activation was significantly (p<0.0001) increased in BG-treated cells compared to controls (**Figs. 6B & 6C**). Recent studies have demonstrated that shorter WPB are associated with reductions in high molecular weight multimers (HMWM) and attenuated hemostatic capacity of secreted VWF to capture platelets on the surface of activated EC.[42,43] Consistently, we observed reduced HMWM in conditioned media from BG-treated HUVEC compared to untreated controls (**Fig. 6D**). Moreover, VWF collagen binding activity (VWF:CB) was also significantly reduced

(p=0.0223) for VWF secreted from BG-treated cells under steady state conditions, or in response to histamine activation (**Fig. 6E**).

In keeping with the reduction in WPB size, BG treatment of HUVEC was also associated with a significant reduction (p=0.0002) in total VWF:Ag secreted after histamine stimulation. (**Fig. 7A**). To further elucidate the effects of OLG inhibition in human EC on VWF biology, we next investigated the formation of tethered VWF strings, and platelet-decorated VWF strings, on the surface of histamine-activated HUVEC under shear conditions (**Fig. 7B**). Consistent with the reduction in WPB length, platelet-decorated VWF strings on the surface activated HUVEC were significantly (p<0.0001) shorter following BG treatment (**Figs. 7C & 7D**). Furthermore, we observed that fluorescently labeled VWF strings from BG-treated HUVEC following histamine stimulation were also significantly reduced in length (**Figs. 7E & 7F**). Collectively, these findings confirm that OLG truncation significantly influences VWF activation, multimerization and the ability of VWF to capture platelets on the surface of activated EC.

DISCUSSION

O-glycan determinants have been implicated in regulating several key aspects of VWF biology.[12,13] For example, previous studies performed following tail vein injection in *VWF*$^{-/-}$ mice and rats consistently reported that loss of OLG was associated with a significant reduction in VWF plasma half-life.[20,28] Subsequent studies have confirmed that sialylation on OLG plays a critical role in protecting VWF against rapid clearance mediated via the macrophage galactose lectin (MGL).[49,50] Conversely, previous studies investigating whether OLG influences VWF biosynthesis reached differing conclusions.[27-29] Nowak *et al* performed alanine mutagenesis to remove OLG sites in human VWF individually or in combination, and then studied rVWF expression in HEK293**T** cells.[27] In this model, no significant OLG effects on rVWF synthesis or secretion were observed. Conversely, Badirou *et al* investigated the significance of OLG by performing mutagenesis to remove OLG sites in murine rVWF and then assessed expression by either hydrodynamic expression in *VWF*$^{-/-}$ mice,[28,51] or following transient transfection of Cos-7 cells.[28] In contrast to Nowak *et al*, they reported that loss of OLG was associated with a significant reduction in rVWF expression. These differences likely relate in large part to the fact that the studies involved human and murine rVWF variants expressed in different cell lines (HEK293T cells, murine primary hepatocytes and Cos-7 cells).

In this study we adopted a different strategy to investigate a putative role for OLG in regulating VWF biosynthesis using O-glycosylation inhibitors in human endothelial cells (HUVEC). This approach is similar to the original studies that showed that NLG sugars influence VWF trafficking and secretion.[26,52] Our HUVEC findings demonstrate that OLG

truncation on VWF leads to a significant reduction in WPB length, an increase in VWF steady-state secretion and a reduction in VWF exocytosis following EC activation. Consistent with these HUVEC data, expression of rVWF variants lacking OLG clusters flanking the VWF-A1 domain also resulted in the formation of significantly shortened pseudo-WPB in HEK293 cells compared to those seen following VWF-WT expression. Together these data suggest that the OLG structures, particularly the cluster located on the N-terminal side of the VWF-A1 domain, directly influence WPB formation. Recent studies have demonstrated that WPB length can be similarly reduced by a variety of agents (including statins and nocodazole) that lead to unlinking of the Golgi ribbon into ministack.[42-44] However, we observed no significant change in Golgi in HUVEC following OLG truncation. Consequently, it seems likely that OLG truncation may instead affect the availability of VWF quanta for packing into nascent WPB.

The mechanism(s) through which OLG truncation influences VWF secretion and WPB morphology remain to be fully elucidated. However, previous studies have shown that the N- and C-terminal flanking regions of the A1 domain cooperatively form an autoinhibitory module (AIM) that reduces accessibility to the GPIbα binding site located within the VWF-A1 domain.[53-55] Notably, OLG structures are present in both the N-AIM and C-AIM regions and are largely conserved in mammals.[47] Interestingly, Vos *et al* recently reported that desialylation of OLG chains located within the AIM regions leads to destabilization of the autoinhibitory effect and VWF-A1 domain activation.[47] In keeping with the hypothesis that OLG influence AIM, we further demonstrate that BG-induced loss of O-linked sialylation also results in VWF-A1 activation in human EC. Thus, in contrast to the previous mutagenesis studies which involved loss of complete

OLG chains,[27,28] our findings highlight that relatively modest changes in OLG structures, such as reductions in terminal α2-3 sialylation, have the potential to significantly influence multiple aspects of VWF biosynthesis and secretion.

Previous OLG mutagenesis studies did not observe any effect on VWF multimerization for rVWF variants compared to VWF-WT expressed in the same cells.[27-29] However, those VWF expression studies were performed in murine hepatocytes and HEK293T cells in which expression of HMWM was limited. Conversely, following BG-treatment of HUVEC, we observed a significant decrease in HMWM and a consistent reduction in VWF:CB activity. These findings are interesting given that very recent electron cryo-microscopy studies have reported a novel direct role for the VWF-A1 domain in directing VWF tubule formation and concatamerization.[56,57] In addition, we observed that OLG truncation was associated with a significant reduction in the length of tethered platelet-decorated VWF strings on the surface of activated ECs under flow. This finding is consistent with previous reports showing that unlinking of the Golgi ribbon with simvastatin or nocodazole treatment not only led to a reduction in WPB size, but also to the formation of significantly shorter VWF strings.[42-44] Together, these findings raise the intriguing possibility that therapeutic modulation of WPB organelle size might offer a novel approach to antithrombotic therapy.[44]

From a clinical perspective, it is important to highlight that reduced VWF biosynthesis and secretion have been shown to constitute the most common pathogenic mechanism in patients with type 1 VWD (plasma VWF:Ag levels < 30 IU/dL) and Low VWF (plasma VWF levels 30-50 IU/dL) respectively.[58-61] Furthermore, van Schooten *et al* demonstrated that binding of the lectin PNA to plasma VWF was significantly enhanced

in a significant subgroup of type 1 VWD patients compared to healthy controls.[62] These lectin data suggest that O-linked T antigen expression on plasma VWF is significantly increased in these patients. Our data show that increased T antigen expression on VWF can influence multiple aspects of EC biosynthesis and secretion. Importantly, the RIIIS/J mouse provides a naturally occurring proof-of-principle that glycosylation abnormalities targeted specifically to EC can directly cause VWD without necessarily leading to other multi-system pleiotropic effects.[63] This in-bred strain of mice has significantly reduced plasma VWF levels compared to other murine strains and consequently displays a bleeding phenotype. Previous studies have demonstrated that reduced plasma VWF levels in RIIIS/J mice are due to aberrant expression of an N-acetylglactosaminyltransferase in EC, which results in altered VWF glycosylation and consequently pathological enhanced VWF clearance.[63] Critically however, RIIIS/J mice with this EC-specific glycosylation abnormality do not have multisystem abnormalities like those typically observed in patients with Congenital Disorders of Glycosylation (CDG).[64,65] Further studies will be required to elucidate the biological mechanism(s) underpinning the increase in O-linked T antigen expression in type 1 VWD patients. These studies will be complicated by the fact that there is significant inter-individual heterogeneity in VWF glycosylation in both normal people and in VWD patients.[23] Furthermore, alterations in VWF sialylation may occur during EC biosynthesis, or following digestion by circulating neuraminidases present in the plasma.[23,66] Nevertheless, we hypothesize that alterations in O-linked glycosylation or sialylation machinery within EC could contribute to the pathogenesis of VWD, particularly in families in whom the disease is not linked to the *VWF* locus on chromosome 12.

Acknowledgements

J.S.O.D. is supported by funds from the NIH for the Zimmerman Program (HL081588) and a Science Foundation Ireland Principal Frontiers for the Future (FFP) award (20/FFP-A/8952). The authors would like to acknowledge RCSI's Super-Resolution Image Consortium (SRIC) facility funded by Science Foundation Ireland (18/RI/5723).

Authorship

E.K. and J.S.O.D conceived the study and contributed to data collection and interpretation. D.D., P.B., M.G. and S.E assisted with data collection. I.S. assisted with image analysis. E.K., D.D., P.B., M.G., S.E., R.B., and J.S.O.D. contributed to the literature review, final draft writing, and critical revision and approved the final version of the manuscript. All the authors have participated sufficiently in this work, take public responsibility for the content, and have made substantial contributions to this research.

Conflict-of-interest disclosure:

J.S.O.D has served on the speaker's bureau for Baxter, Bayer, Novo Nordisk, Sobi, Boehringer Ingelheim, Leo Pharma, Takeda and Octapharma. He has also served on the advisory boards of Baxter, Sobi, Bayer, Octapharma CSL Behring, Daiichi Sankyo, Boehringer Ingelheim, Takeda and Pfizer. J.S.O.D has also received research grant funding awards from 3M, Baxter, Bayer, Pfizer, Shire, Takeda, 3M and Novo Nordisk. The remaining authors have no conflict-of-interests to declare.

REFERENCES

1. Leebeek FW, Eikenboom JC. Von Willebrand's Disease. *N Engl J Med*. 2016;375(21):2067-2080.

2. Wagner DD. Cell biology of von Willebrand factor. *Annu Rev Cell Biol*. 1990;6:217-246.

3. Lenting PJ, Christophe OD, Denis CV. von Willebrand factor biosynthesis, secretion, and clearance: connecting the far ends. *Blood*. 2015;125(13):2019-2028.

4. Preston RJ, Rawley O, Gleeson EM, O'Donnell JS. Elucidating the role of carbohydrate determinants in regulating hemostasis: insights and opportunities. *Blood*. 2013;121(19):3801-3810.

5. Titani K, Kumar S, Takio K, et al. Amino acid sequence of human von Willebrand factor. *Biochemistry*. 1986;25(11):3171-3184.

6. Canis K, McKinnon TA, Nowak A, et al. Mapping the N-glycome of human von Willebrand factor. *Biochem J*. 2012;447(2):217-228.

7. Brockhausen I, Schutzbach J, Kuhns W. Glycoproteins and their relationship to human disease. *Acta Anat (Basel)*. 1998;161(1-4):36-78.

8. Ju T, Otto VI, Cummings RD. The Tn antigen-structural simplicity and biological complexity. *Angew Chem Int Ed Engl*. 2011;50(8):1770-1791.

9. Hanisch FG. O-glycosylation of the mucin type. *Biol Chem*. 2001;382(2):143-149.

10. Canis K, McKinnon TA, Nowak A, et al. The plasma von Willebrand factor O-glycome comprises a surprising variety of structures including ABH antigens and disialosyl motifs. *J Thromb Haemost*. 2010;8(1):137-145.

11. Solecka BA, Weise C, Laffan MA, Kannicht C. Site-specific analysis of von Willebrand factor O-glycosylation. *J Thromb Haemost*. 2016;14(4):733-746.

12. Ward S, O'Sullivan JM, O'Donnell JS. The Biological Significance of von Willebrand Factor O-Linked Glycosylation. *Semin Thromb Hemost*. 2021;47(7):855-861.

13. Ward S, O'Sullivan JM, O'Donnell JS. von Willebrand factor sialylation-A critical regulator of biological function. *J Thromb Haemost*. 2019;17(7):1018-1029.

14. Ward SE, O'Sullivan JM, O'Donnell JS. The relationship between ABO blood group, von Willebrand factor, and primary hemostasis. *Blood*. 2020;136(25):2864-2874.

15. Bowen DJ. An influence of ABO blood group on the rate of proteolysis of von Willebrand factor by ADAMTS13. *J Thromb Haemost*. 2003;1(1):33-40.

16. McGrath RT, van den Biggelaar M, Byrne B, et al. Altered glycosylation of platelet-derived von Willebrand factor confers resistance to ADAMTS13 proteolysis. *Blood*. 2013;122(25):4107-4110.

17. McGrath RT, McKinnon TA, Byrne B, et al. Expression of terminal alpha2-6-linked sialic acid on von Willebrand factor specifically enhances proteolysis by ADAMTS13. *Blood*. 2010;115(13):2666-2673.

18. McKinnon TA, Chion AC, Millington AJ, Lane DA, Laffan MA. N-linked glycosylation of VWF modulates its interaction with ADAMTS13. *Blood*. 2008;111(6):3042-3049.

19. Sodetz JM, Pizzo SV, McKee PA. Relationship of sialic acid to function and in vivo survival of human factor VIII/von Willebrand factor protein. *J Biol Chem*. 1977;252(15):5538-5546.

20. Stoddart JH, Jr., Andersen J, Lynch DC. Clearance of normal and type 2A von Willebrand factor in the rat. *Blood*. 1996;88(5):1692-1699.

21. Grewal PK, Uchiyama S, Ditto D, et al. The Ashwell receptor mitigates the lethal coagulopathy of sepsis. *Nat Med*. 2008;14(6):648-655.

22. O'Sullivan JM, Aguila S, McRae E, et al. N-linked glycan truncation causes enhanced clearance of plasma-derived von Willebrand factor. *J Thromb Haemost*. 2016;14(12):2446-2457.

23. Aguila S, Lavin M, Dalton N, et al. Increased galactose expression and enhanced clearance in patients with low von Willebrand factor. *Blood*. 2019;133(14):1585-1596.

24. Chion A, O'Sullivan JM, Drakeford C, et al. N-linked glycans within the A2 domain of von Willebrand factor modulate macrophage-mediated clearance. *Blood*. 2016;128(15):1959-1968.

25. Wagner DD, Mayadas T, Marder VJ. Initial glycosylation and acidic pH in the Golgi apparatus are required for multimerization of von Willebrand factor. *J Cell Biol*. 1986;102(4):1320-1324.

26. McKinnon TA, Goode EC, Birdsey GM, et al. Specific N-linked glycosylation sites modulate synthesis and secretion of von Willebrand factor. *Blood*. 2010;116(4):640-648.

27. Nowak AA, Canis K, Riddell A, Laffan MA, McKinnon TA. O-linked glycosylation of von Willebrand factor modulates the interaction with platelet receptor glycoprotein Ib under static and shear stress conditions. *Blood*. 2012;120(1):214-222.

28. Badirou I, Kurdi M, Legendre P, et al. In vivo analysis of the role of O-glycosylations of von Willebrand factor. *PLoS One*. 2012;7(5):e37508.

29. Carew JA, Quinn SM, Stoddart JH, Lynch DC. O-linked carbohydrate of recombinant von Willebrand factor influences ristocetin-induced binding to platelet glycoprotein 1b. *J Clin Invest*. 1992;90(6):2258-2267.

30. Michaux G, Hewlett LJ, Messenger SL, et al. Analysis of intracellular storage and regulated secretion of 3 von Willebrand disease-causing variants of von Willebrand factor. *Blood*. 2003;102(7):2452-2458.

31. Sabater-Lleal M, Huffman JE, de Vries PS, et al. Genome-Wide Association Transethnic Meta-Analyses Identifies Novel Associations Regulating Coagulation Factor VIII and von Willebrand Factor Plasma Levels. *Circulation*. 2019;139(5):620-635.

32. Gouyer V, Leteurtre E, Delmotte P, et al. Differential effect of GalNAcalpha-O-bn on intracellular trafficking in enterocytic HT-29 and Caco-2 cells: correlation with the glycosyltransferase expression pattern. *J Cell Sci*. 2001;114(Pt 8):1455-1471.

33. O'Donnell J, Boulton FE, Manning RA, Laffan MA. Amount of H antigen expressed on circulating von Willebrand factor is modified by ABO blood group genotype and is a major determinant of plasma von Willebrand factor antigen levels. *Arterioscler Thromb Vasc Biol*. 2002;22(2):335-341.

34. Swinkels M, Atiq F, Burgisser PE, et al. Quantitative 3D microscopy highlights altered von Willebrand factor alpha-granule storage in patients with von Willebrand disease with distinct pathogenic mechanisms. *Res Pract Thromb Haemost*. 2021;5(6):e12595.

35. Fogarty H, Ward SE, Townsend L, et al. Sustained VWF-ADAMTS-13 axis imbalance and endotheliopathy in long COVID syndrome is related to immune dysfunction. *J Thromb Haemost*. 2022;20(10):2429-2438.

36. Wohner N, Sebastian S, Muczynski V, et al. Osteoprotegerin modulates platelet adhesion to von Willebrand factor during release from endothelial cells. *J Thromb Haemost*. 2022;20(3):755-766.

37. Kenny M, Stamboroski S, Taher R, Bruggemann D, Schoen I. Nanofiber Topographies Enhance Platelet-Fibrinogen Scaffold Interactions. *Adv Healthc Mater*. 2022;11(14):e2200249.

38. Delannoy P, Kim I, Emery N, et al. Benzyl-N-acetyl-alpha-D-galactosaminide inhibits the sialylation and the secretion of mucins by a mucin secreting HT-29 cell subpopulation. *Glycoconj J*. 1996;13(5):717-726.

39. Byrd JC, Dahiya R, Huang J, Kim YS. Inhibition of mucin synthesis by benzyl-alpha-GalNAc in KATO III gastric cancer and Caco-2 colon cancer cells. *Eur J Cancer*. 1995;31A(9):1498-1505.

40. Lin MC, Chien PH, Wu HY, et al. C1GALT1 predicts poor prognosis and is a potential therapeutic target in head and neck cancer. *Oncogene*. 2018;37(43):5780-5793.

41. Sun X, Zhan M, Sun X, Liu W, Meng X. C1GALT1 in health and disease. *Oncol Lett*. 2021;22(2):589.

42. Ferraro F, Kriston-Vizi J, Metcalf DJ, et al. A two-tier Golgi-based control of organelle size underpins the functional plasticity of endothelial cells. *Dev Cell*. 2014;29(3):292-304.

43. Ferraro F, Mafalda Lopes da S, Grimes W, et al. Weibel-Palade body size modulates the adhesive activity of its von Willebrand Factor cargo in cultured endothelial cells. *Sci Rep*. 2016;6:32473.

44. Ferraro F, Patella F, Costa JR, Ketteler R, Kriston-Vizi J, Cutler DF. Modulation of endothelial organelle size as an antithrombotic strategy. *J Thromb Haemost*. 2020;18(12):3296-3308.

45. Karampini E, Fogarty H, Elliott S, et al. Endothelial cell activation, Weibel-Palade body secretion, and enhanced angiogenesis in severe COVID-19. *Res Pract Thromb Haemost*. 2023;7(2):100085.

46. Fogarty H, Ahmad A, Atiq F, et al. VWF-ADAMTS13 axis dysfunction in children with sickle cell disease treated with hydroxycarbamide vs blood transfusion. *Blood Adv*. 2023;7(22):6974-6989.

47. Voos KM, Cao W, Arce NA, et al. Desialylation of O-glycans activates von Willebrand factor by destabilizing its autoinhibitory module. *J Thromb Haemost*. 2022;20(1):196-207.

48. Hulstein JJ, de Groot PG, Silence K, Veyradier A, Fijnheer R, Lenting PJ. A novel nanobody that detects the gain-of-function phenotype of von Willebrand factor in ADAMTS13 deficiency and von Willebrand disease type 2B. *Blood*. 2005;106(9):3035-3042.

49. Ward SE, O'Sullivan JM, Drakeford C, et al. A novel role for the macrophage galactose-type lectin receptor in mediating von Willebrand factor clearance. *Blood*. 2018;131(8):911-916.

50. Ward SE, O'Sullivan JM, Moran AB, et al. Sialylation on O-linked glycans protects von Willebrand factor from macrophage galactose lectin mediated clearance. *Haematologica*. 2021.

51. Pruss CM, Golder M, Bryant A, et al. Pathologic mechanisms of type 1 VWD mutations R1205H and Y1584C through in vitro and in vivo mouse models. *Blood*. 2011;117(16):4358-4366.

52. Wagner DD, Marder VJ. Biosynthesis of von Willebrand protein by human endothelial cells: processing steps and their intracellular localization. *J Cell Biol*. 1984;99(6):2123-2130.

53. Deng W, Voos KM, Colucci JK, et al. Delimiting the autoinhibitory module of von Willebrand factor. *J Thromb Haemost*. 2018;16(10):2097-2105.

54. Deng W, Wang Y, Druzak SA, et al. A discontinuous autoinhibitory module masks the A1 domain of von Willebrand factor. *J Thromb Haemost*. 2017;15(9):1867-1877.

55. Arce NA, Cao W, Brown AK, et al. Activation of von Willebrand factor via mechanical unfolding of its discontinuous autoinhibitory module. *Nat Commun*. 2021;12(1):2360.

56. Anderson JR, Li J, Springer TA, Brown A. Structures of VWF tubules before and after concatemerization reveal a mechanism of disulfide bond exchange. *Blood*. 2022;140(12):1419-1430.

57. Javitt G, Yeshaya N, Khmelnitsky L, Fass D. Assembly of von Willebrand factor tubules with in vivo helical parameters requires A1 domain insertion. *Blood*. 2022;140(26):2835-2843.

58. Flood VH, Christopherson PA, Gill JC, et al. Clinical and laboratory variability in a cohort of patients diagnosed with type 1 VWD in the United States. *Blood*. 2016;127(20):2481-2488.

59. Lavin M, Aguila S, Schneppenheim S, et al. Novel insights into the clinical phenotype and pathophysiology underlying low VWF levels. *Blood*. 2017;130(21):2344-2353.

60. Atiq F, Blok R, van Kwawegen C, et al. Type 1 VWD classification revisited - novel insights from combined analysis of the LoVIC and WiN studies. *Blood*. 2023.

61. O'Donnell JS. Low VWF: insights into pathogenesis, diagnosis, and clinical management. *Blood Adv*. 2020;4(13):3191-3199.

62. van Schooten CJ, Denis CV, Lisman T, et al. Variations in glycosylation of von Willebrand factor with O-linked sialylated T antigen are associated with its plasma levels. *Blood*. 2007;109(6):2430-2437.

63. Mohlke KL, Purkayastha AA, Westrick RJ, et al. Mvwf, a dominant modifier of murine von Willebrand factor, results from altered lineage-specific expression of a glycosyltransferase. *Cell*. 1999;96(1):111-120.

64. Francisco R, Brasil S, Poejo J, et al. Congenital disorders of glycosylation (CDG): state of the art in 2022. *Orphanet J Rare Dis*. 2023;18(1):329.

65. Lefeber DJ, Freeze HH, Steet R, Kinoshita T. Congenital Disorders of Glycosylation. In: Varki A, Cummings RD, Esko JD, et al., eds. Essentials of Glycobiology. Cold Spring Harbor (NY); 2022:599-614.

66. Yang WH, Aziz PV, Heithoff DM, Mahan MJ, Smith JW, Marth JD. An intrinsic mechanism of secreted protein aging and turnover. *Proc Natl Acad Sci U S A*. 2015;112(44):13657-13662.

FIGURE LEGENDS

Figure 1. BG treatment of HUVECs alters VWF O-linked glycosylation.

[A]. Inhibitory effect of Benzyl-N-acetyl-galactosaminide (BG) on O-glycan biosynthetic processing; [**B]**. VWF immunoblot in HUVEC cell lysates and conditioned media after BG treatment (GAPDH loading control; representative blot of n=3); **[C]**. *Maackia amurensis* lectin *II* (MAL-II) binding to VWF secreted from BG-treated versus untreated HUVEC controls cells (CTRL) (mean and SEM, n=4, simple linear regression, p<0.0001); **[D]**. Peanut agglutinin (PNA) lectin binding to VWF secreted from BG-treated versus untreated HUVEC controls cells (CTRL) (mean and SEM, n=4, simple linear regression, p=0.0063).

Figure 2. O-linked sialylation influences VWF secretion and alters WPB morphology.

[A]. Unstimulated VWF:Ag secretion levels from HUVEC incubated with or without BG (2 mM for 72 hours) (n=8 from 4 independent experiments, Welch's t-test, p=0.0013); **[B].** VWF:Ag levels in unstimulated HUVEC cell lysates following treatment with or without BG (n=8 from 4 independent experiments, t-test, p=0.5099); **[C].** Immunofluorescent images of HUVEC treated with BG (2 mM for 72 hours) compared to untreated controls (CTRL = controls, VWF in grey, DAPI in blue; representative images of 3 independent experiments); Scale bars are set at 10 μm for overview images and at 5 μm for the zoomed regions; **[D]**. Automated assessment of WPB length (results are depicted as normalized to CTRL (n=10 images from 3 independent experiments, t-test, p<0.0001); **[E].** Automated assessment of WPB circularity (data are shown as

normalized to CTRL) in CTRL and BG-treated cells (n=10 images from 3 independent experiments, t-test, p<0.0001).

Figure 3. C1GALT1 influences VWF O-linked glycan determinants and WPB morphology.

[A]. Inhibitory effect of itraconazole (ITZ) on O-glycan biosynthetic processing; **[B].** C1GALT1 immunoblot in HUVEC cell lysates after ITZ treatment (α-tubulin loading control; representative blot of n=3); **[C].** VWF immunoblot in HUVEC cell lysates and conditioned media after ITZ treatment (GAPDH loading control; representative blot of n=3); **[D].** Unstimulated VWF:Ag secretion levels from HUVEC incubated with or without ITZ (2μM for 48-72 hours) (n=12 from 4 independent experiments, Mann-Whitney test, p<0.0001); **[E].** Immunofluorescent images of HUVEC treated with ITZ (2μM for 48-72 hours) compared to untreated controls (CTRL = controls, VWF in grey, DAPI in blue; representative images of 3 independent experiments). Scale bars are set at 10 μm for overview images and at 5 μm for the zoomed regions; **[F]**. Automated assessment of WPB length (data are shown as normalized to CTRL) in CTRL and ITZ-treated cells (n=10 images from 3 independent experiments, t-test, p=0.0026).

Figure 4. Effects of VWF OLG truncation on Golgi morphology and WPB cargo storage.

[A]. Immunofluorescent images of VWF (green), TGN46 (red) and DAPI (blue) of BG-treated HUVEC (2 mM for 72 hours) compared to untreated controls (representative images of 2 independent experiments); **[B].** Immunofluorescence images of VWF (green), Angpiopoietin-2 (Angpt-2) (red) and DAPI (blue) of BG-treated HUVEC

compared to untreated control cells (yellow arrowheads indicate WPBs positive for Angpt-2; representative images of n=5); **[C].** Angpt-2 levels secreted into conditioned media from BG-treated HUVEC compared to untreated controls (n=5, t-test, p=0.0062).

Figure 5. O-glycan clusters in VWF impact pseudo-WPB morphology.

[A]. Schematic representation illustrating OLG clustered around the VWF-A1 domain and the recombinant OLG mutants generated; **[B].** Immunofluorescent images of HEK293 cells expressing VWF-WT, VWF-ΔC2, VWF-ΔC1 and VWF-ΔC1+ΔC2. Orange arrowheads in zoomed images point to pseudo-WPBs (representative images of n=3). Scale bars are set at 10 μm for overview images and at 5 μm for the zoomed regions; **[C].** Pseudo-WPB length in VWF-WT, VWF-ΔC2, VWF-ΔC1 and VWF-ΔC1+ΔC2 expressing HEK293 cells (n=3, Kruskal-Wallis test, p=0.01, p<0.0001 and p<0.0001). (n=3 independent experiments). For all images, scale bars are set at 10 μm of overview images and at 5 μm for the zoomed regions, with overview image field containing approximately 20 cells each.

[D]. Pseudo-WPB length in VWF-WT, VWF-WT treated with BG and VWF-ΔC1+ΔC2 expressing HEK293 cells normalized to VWF-WT (n=2 independent experiments, Kruskal-Wallis test with multiple comparisons, p=0.0125, p<0.0001 and p=0.3331); **[E].** Pseudo-WPB length in VWF-ΔC1+ΔC2 and VWF-ΔC1+ΔC2 treated with BG expressing HEK293 cells normalized to VWF-ΔC1+ΔC2 (n=3 independent experiments, Mann-Whitney, p=0.0125, p<0.0001 and p=0.3331).

Figure 6. OLG inhibition leads to VWF-A1 domain activation and reduced HMW multimers.

[A]. Figure illustrates use of nanobodies to detect activated VWF-A1 domain (green: nano-active A1) versus normal VWF-A3 domain (red: nano-A3). [**B]**. Immunofluorescence images of nanobody interactions with BG-treated HUVEC compared to untreated control cells (VWF-A3 in red; active-A1 in green and DAPI in blue; representative images of n=3). Yellow arrowheads point to WPBs positive for both inactive and active VWF. Scale bars are set at 10 μm for overview images and at 5 μm for the zoomed regions; **[C]**. Mean fluorescence intensity (MFI) for nano-active A1 binding in BG-treated HUVEC versus untreated controls (n=22 from 4 independent experiments, Welch's t-test, $p<0.0001$); **[D].** VWF multimer blot and densitometry of conditioned media from BG-treated HUVEC compared to untreated controls (CTRL) (representative images of 2 independent experiments); **[E].** VWF collagen binding activity (VWF:CB) for VWF secreted from HUVEC incubated with or without BG (i) under steady state conditions and (ii) following histamine stimulation (n=6 from 3 independent experiments, one-way ANOVA with multiple comparisons: CTRL vs. BG $p=0.0223$, CTRL his vs BG his $p=0.0223$);

Figure 7. Truncation of OLG causes reduces VWF strings on activated EC.

[A]. VWF:Ag secretion following histamine (100 μM) stimulation from HUVEC incubated with or without BG (n=8 from 4 independent experiments, t-test, $p=0.0086$); **[B].** Histamine activation of HUVECs under shear results in production of tethered VWF strings on the EC surface which can be detected using platelets or fluorescent anti-VWF

antibodies. **[C].** Platelet-decorated VWF string visualized in brightfield after histamine stimulation of BG-treated HUVEC compared to untreated controls (representative images of 2 independent experiments, direction of the flow from top to bottom, flow rate set at 1.5 ml/min (2 dyn/cm^2), scale bars set at 250 pixels); **[D].** Platelet-decorated VWF string length for HUVEC treated with BG compared to untreated control cells (Mann-Whitney test, $p<0.0001$); **[E]**. Fluorescently labelled VWF strings after histamine stimulation of BG-treated HUVEC compared to untreated controls (representative images of 2 independent experiments, direction of the flow from top to bottom, flow rate set at 1.5 ml/min (2 dyn/cm^2) **[F].** Fluorescently labelled VWF string length for HUVEC treated with BG compared to untreated control cells (Mann-Whitney test, $p<0.0001$).

Figure 1

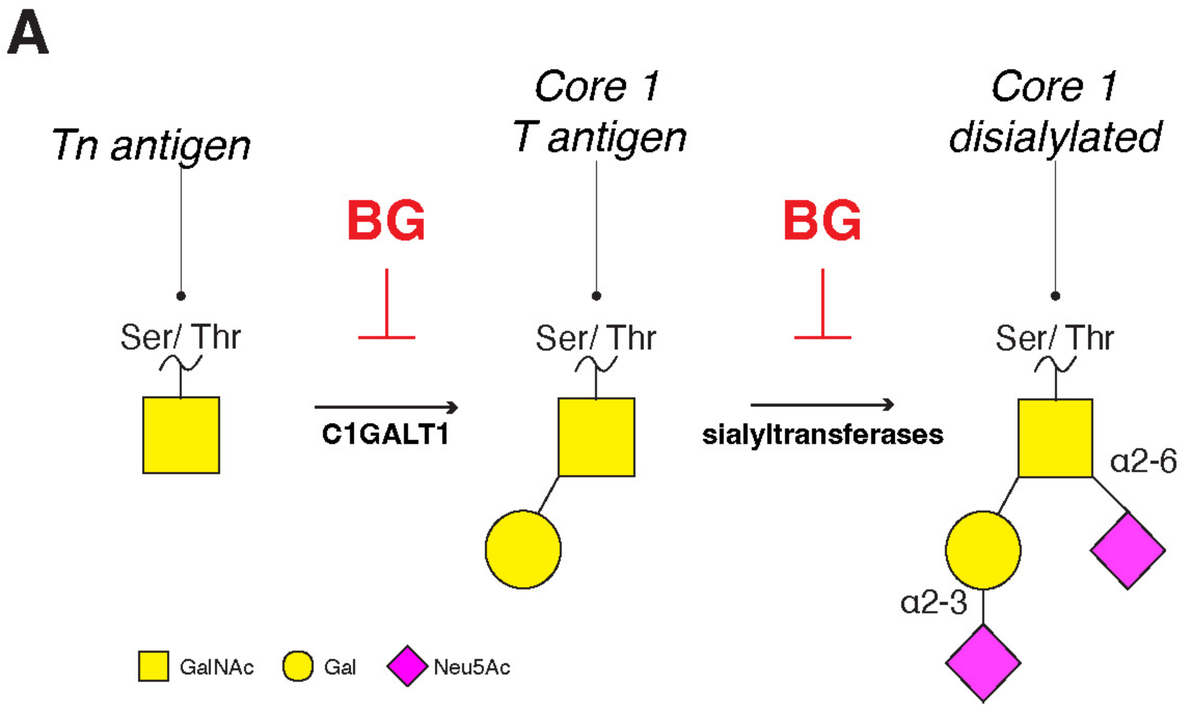

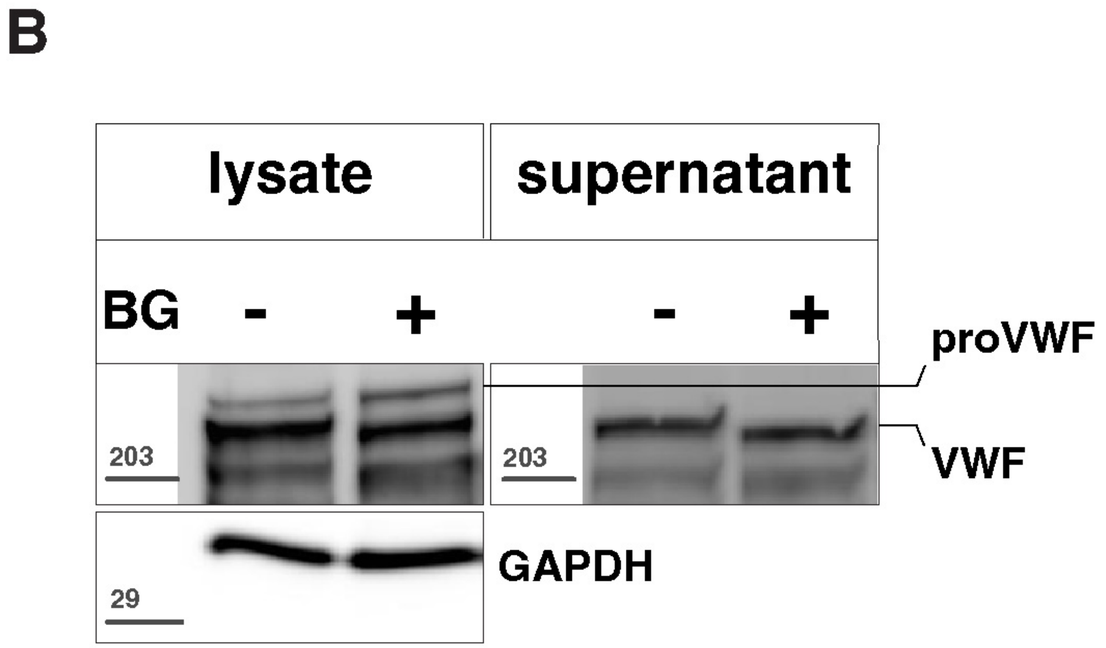

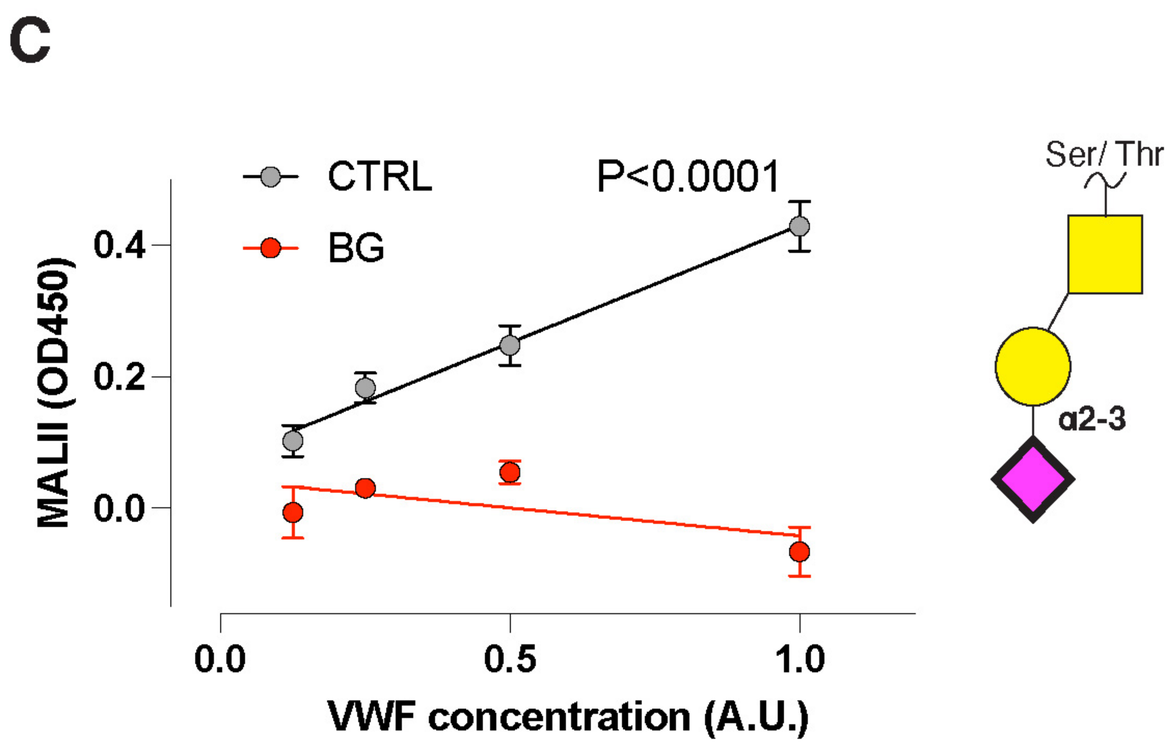

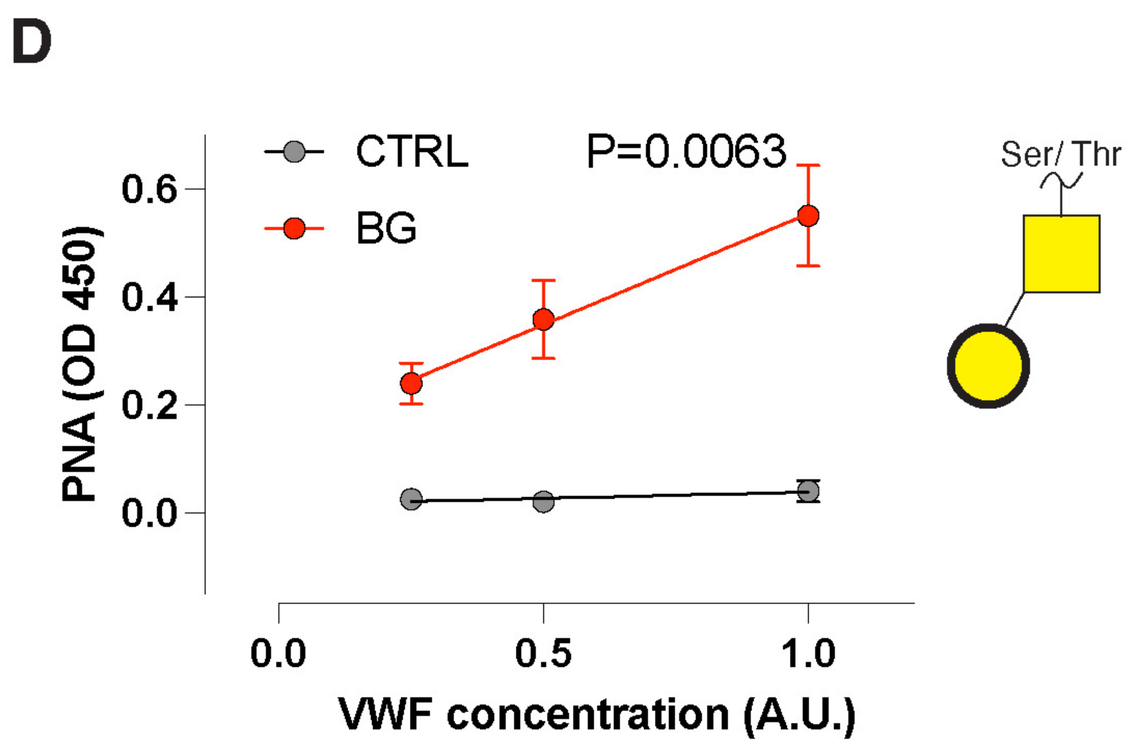

Figure 2

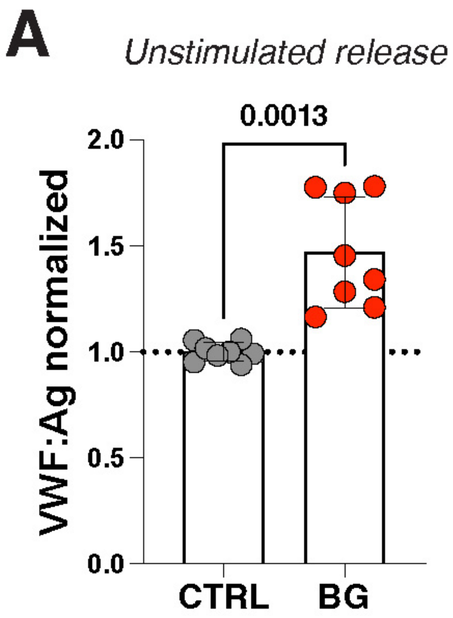

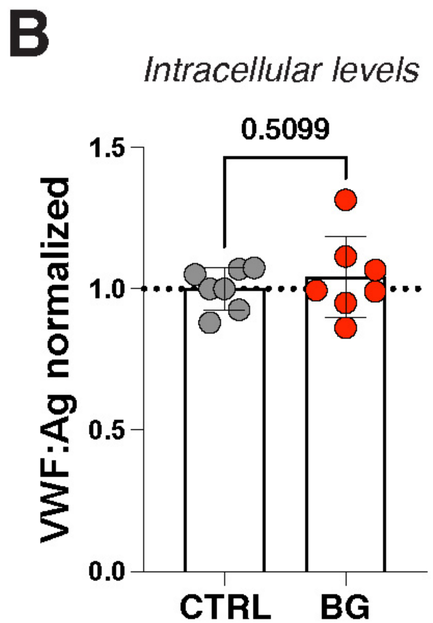

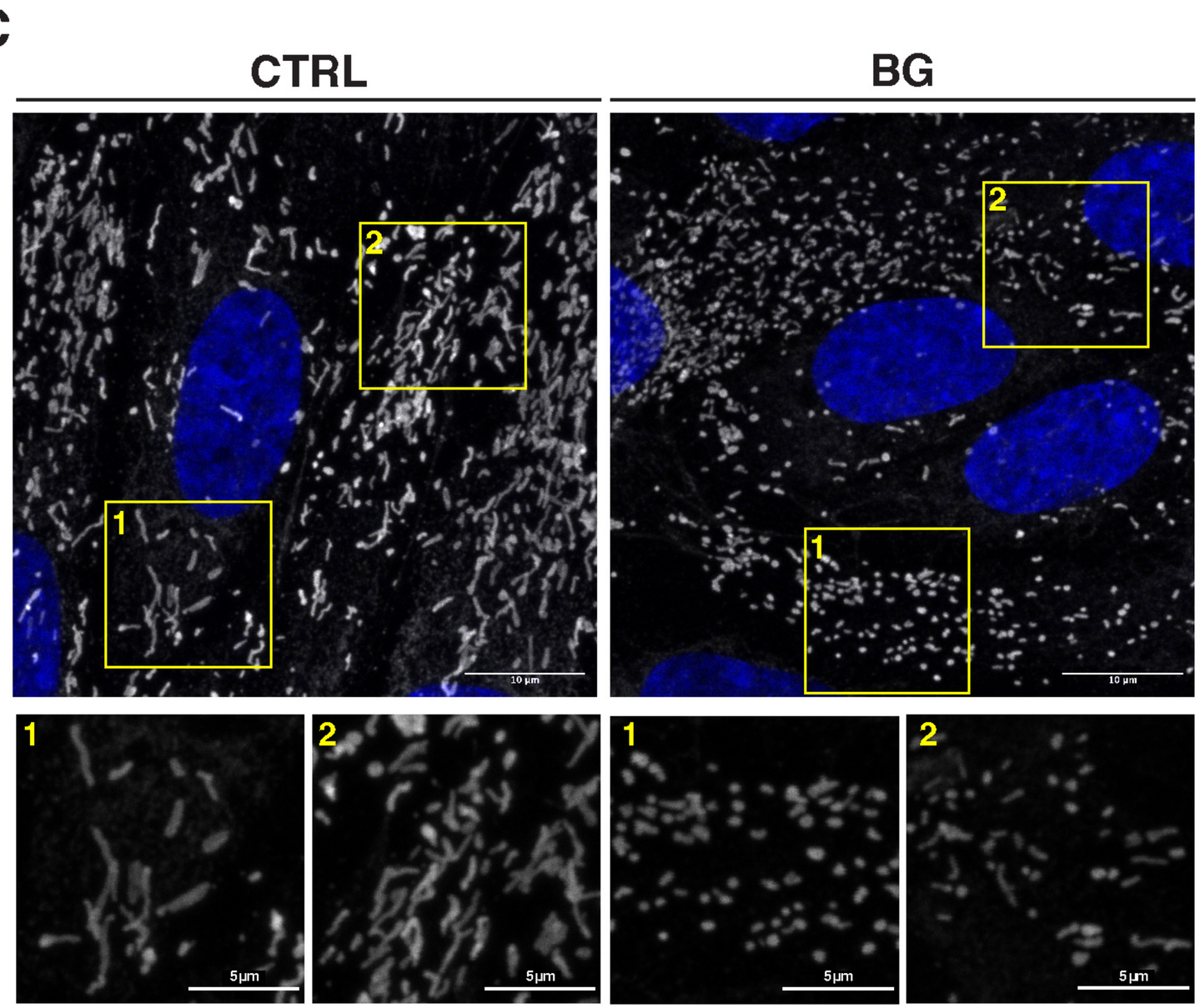

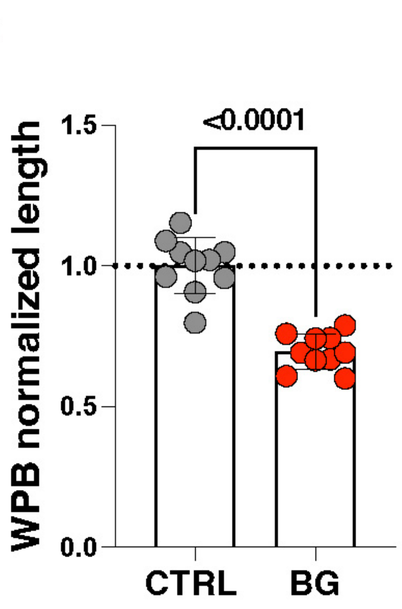

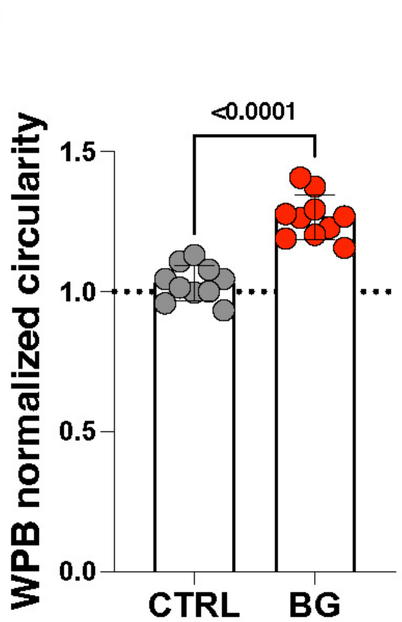

Figure 3

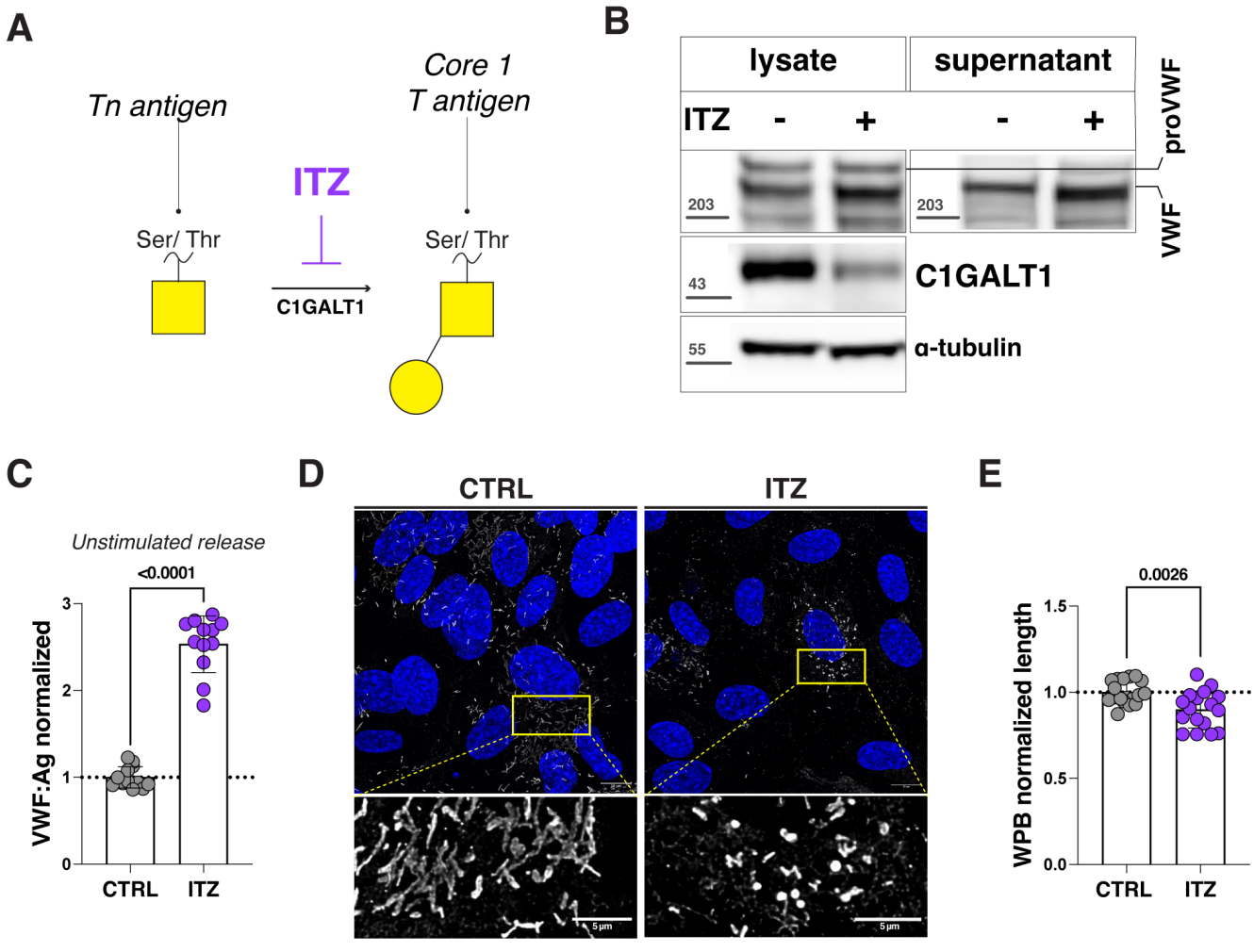

Figure 4

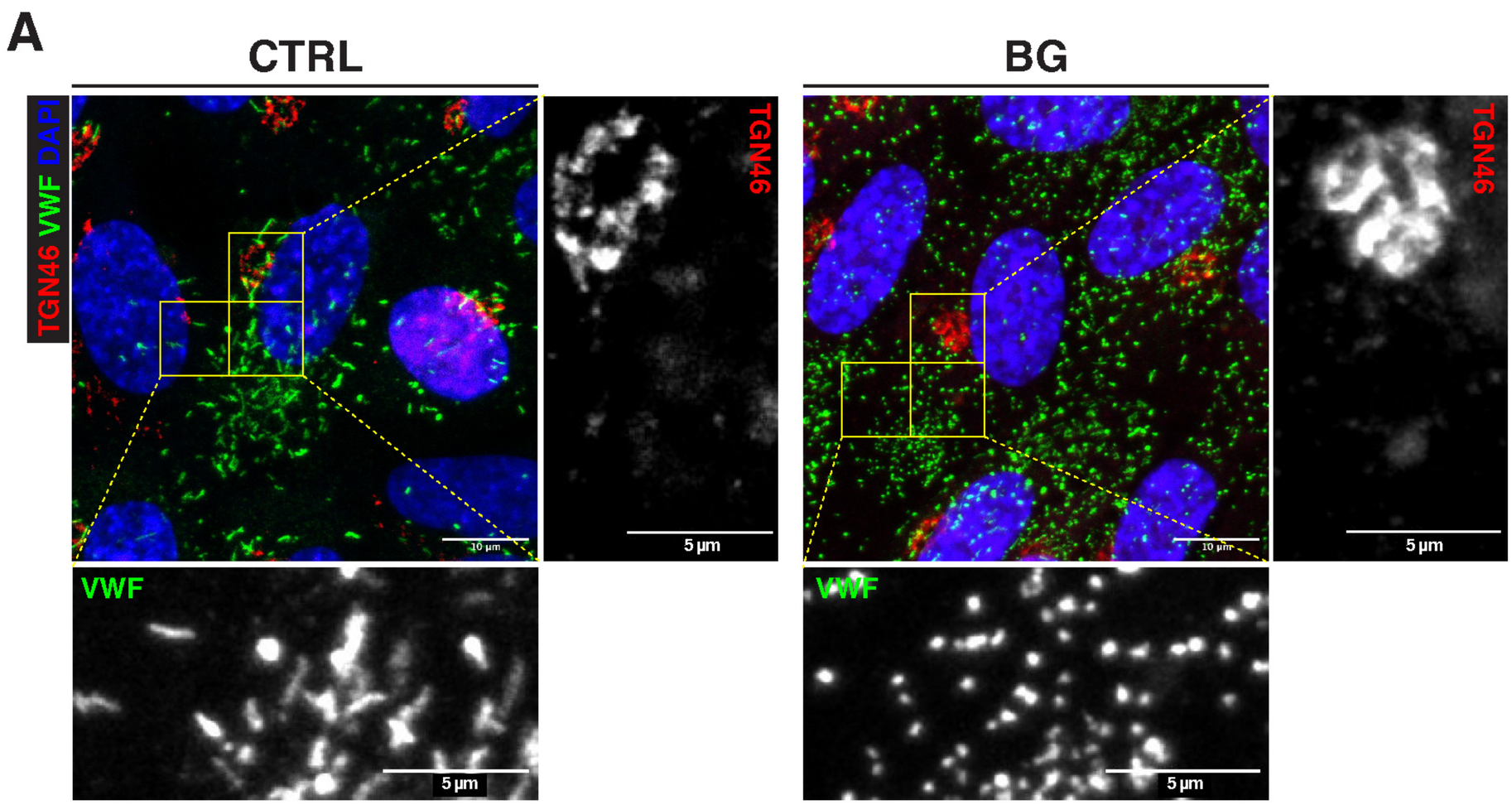

Figure 5

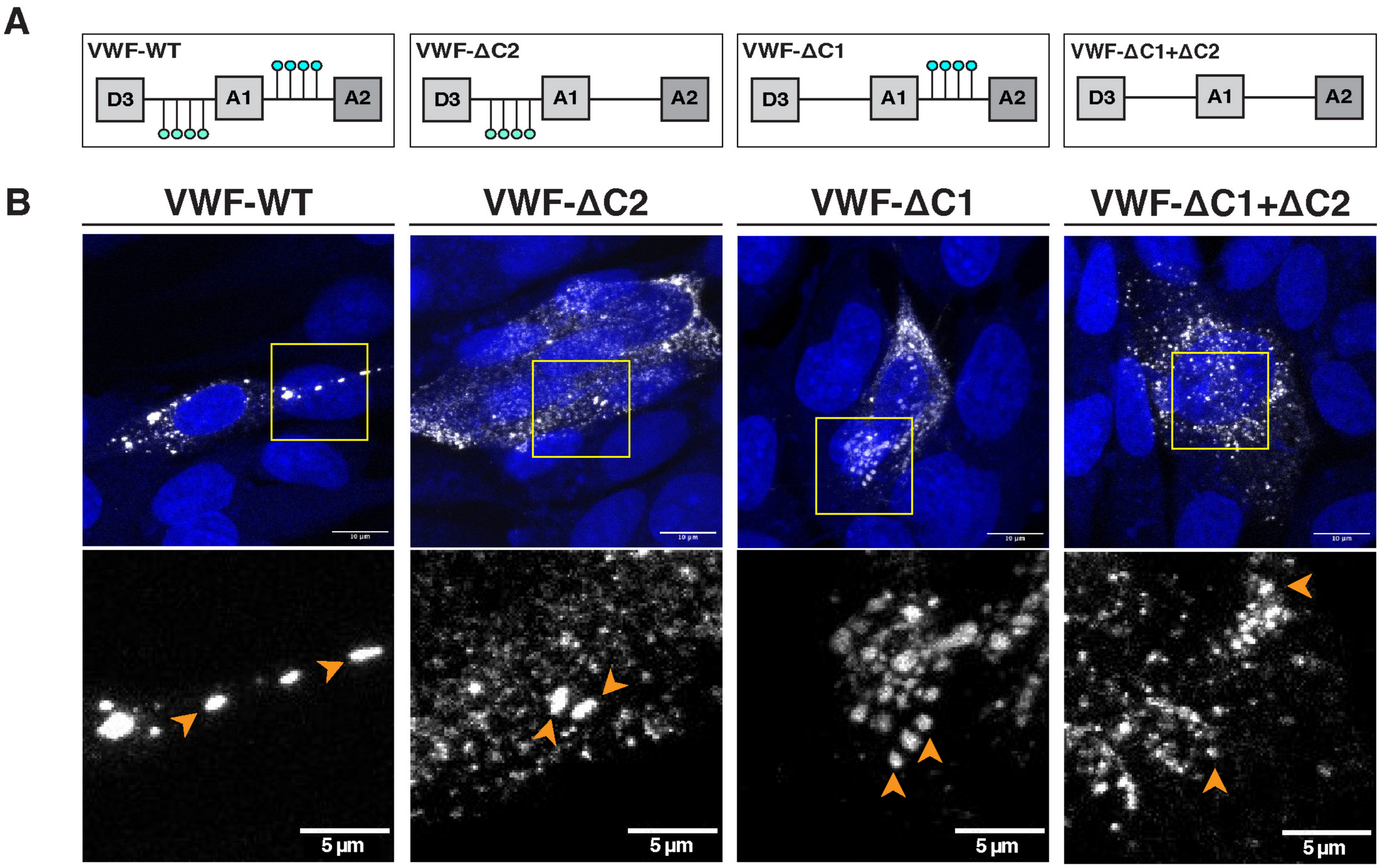

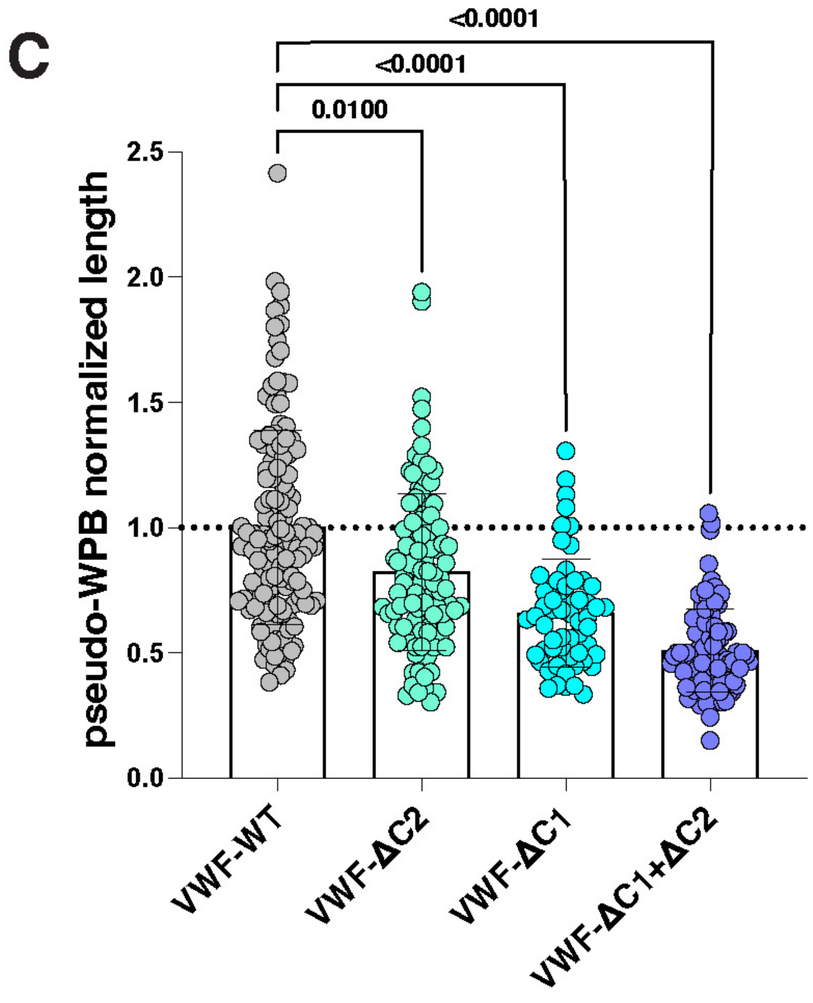

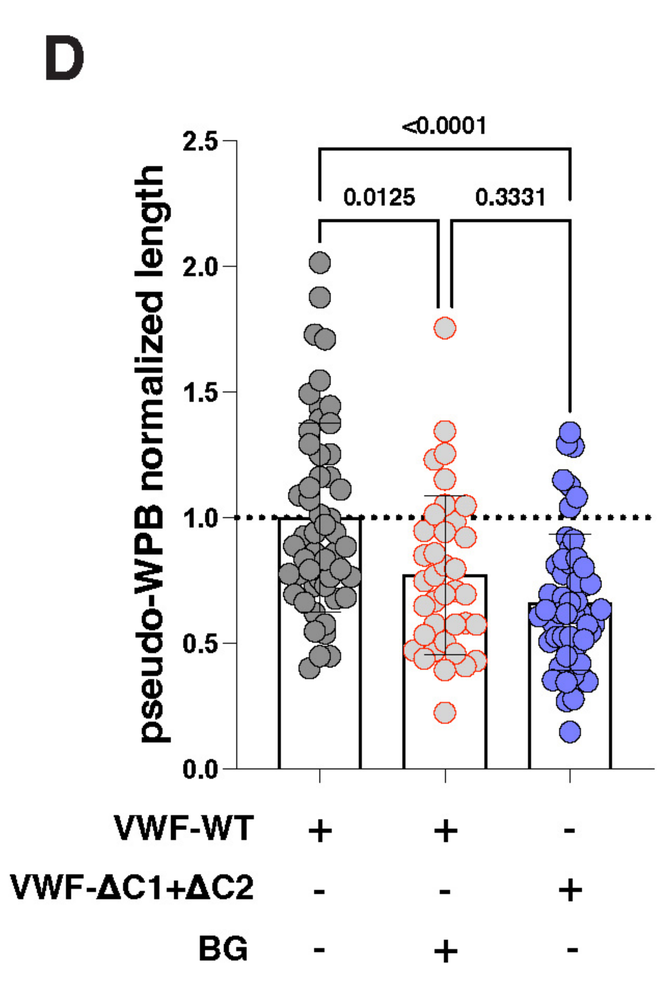

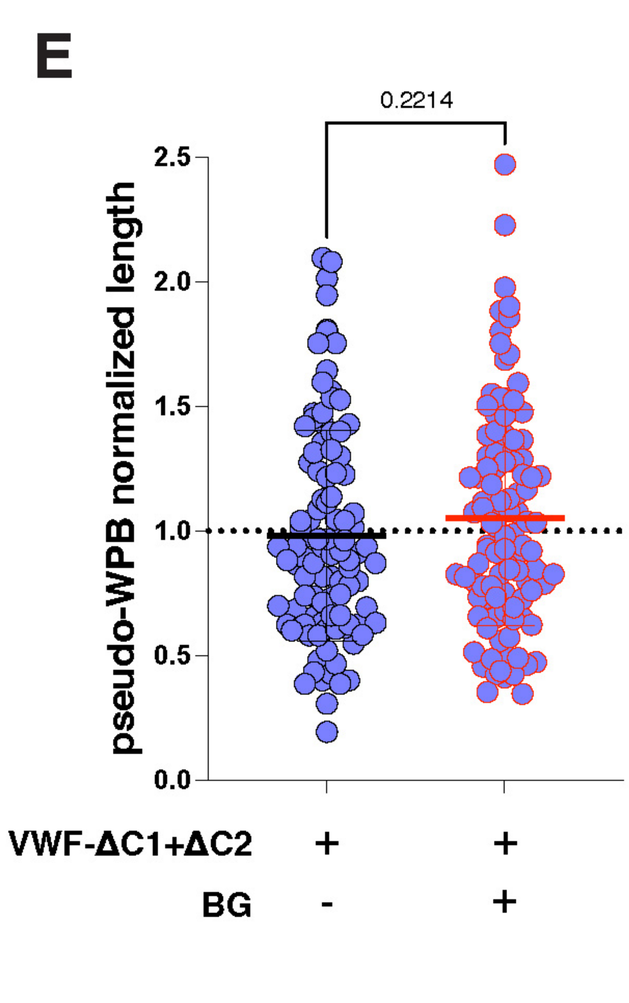

Figure 6

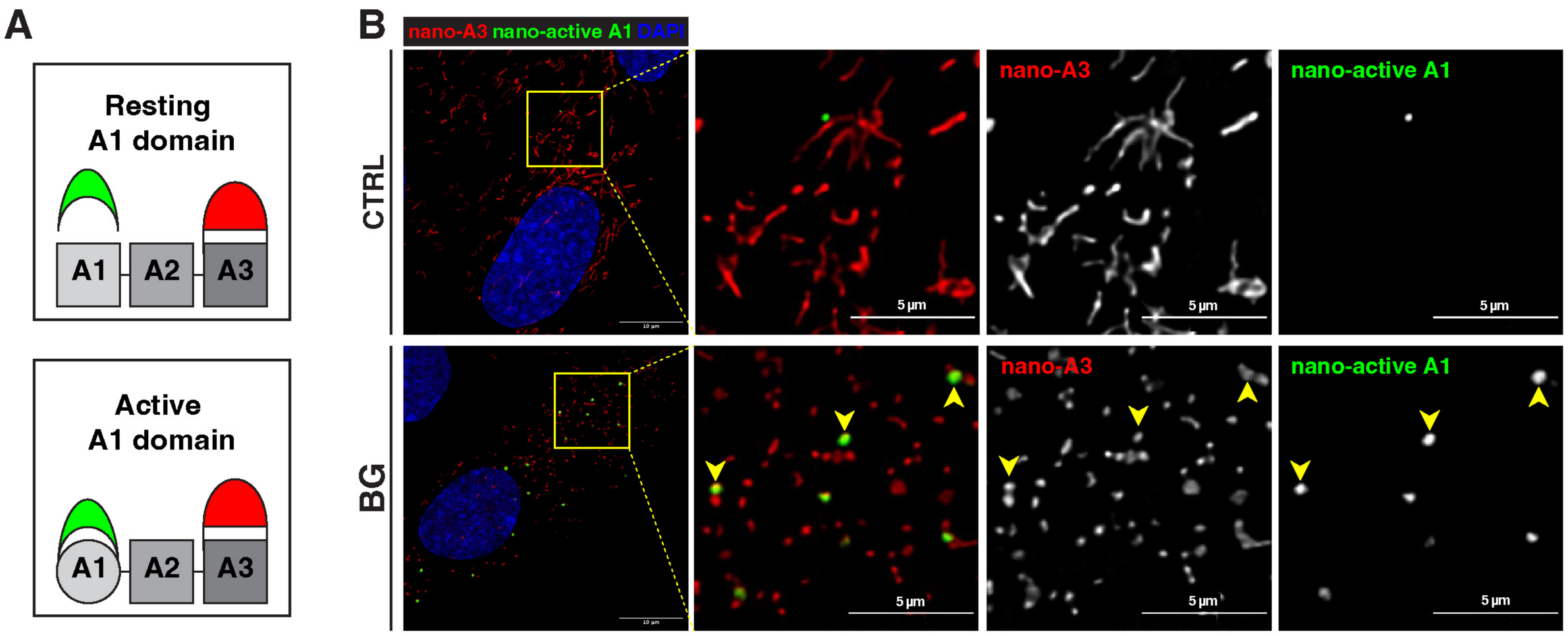
A
Resting
A1 domain
A1
A2
A3
Active
A1 domain
A1
A2
A3
B
nano-A3 nano-active A1 DAPI
CTRL
BG
10 µm
5 µm
nano-A3
nano-active A1
C
<0.0001
normalized
nano-active A1 MFI
0
1
2
CTRL
BG
D
Dimers
LMWM
IMWM
HMWM
UHMWM
CTRL
BG
mean gray value
300
250
200
150
100
50
CTRL
BG
E
0.0223
0.0223
VWF:CB normalized
2.0
1.5
1.0
0.5
0.0
BG
Histamine

Figure 7

A
Histamine stimulation
0.0086
VWF:Ag normalized
1.5
1.0
0.5
0.0
CTRL
BG
B
microfluidic slide
histamine
Ca2+
Ca2+
Direction of flow
platelet decorated VWF strings
fluorescently-labelled VWF strings
C
CTRL
BG
direction of flow
250 pixel
D
<0.0001
platelet-decorated string length normalized
2.0
1.5
1.0
0.5
0.0
CTRL
BG
E
CTRL
BG
direction of flow
100 µm
25 µm
F
<0.0001
fluorescently labelled string length normalized
3.0
2.5
2.0
1.5
1.0
0.5
0.0
CTRL
BG